technologies

MDPI

Article

Full-Wave Simulation of a Helmholtz Radiofrequency Coil for Magnetic Resonance Applications

Giulio Giovannetti [1,*], Denis Burov [2,3], Angelo Galante [4,5,6] and Francesca Frijia [7]

[1] Institute of Clinical Physiology, National Council of Research, 56124 Pisa, Italy
[2] Department of Physical and Chemical Sciences, University of L'Aquila, 67100 L'Aquila, Italy; denis.burov@graduate.univaq.it
[3] Stelar s.r.l., 27035 Mede, Italy
[4] Department of Life, Health & Environmental Sciences, University of L'Aquila, 67100 L'Aquila, Italy; angelo.galante@univaq.it
[5] Gran Sasso National Laboratory, Istituto Nazionale di Fisica Nucleare, 67100 L'Aquila, Italy
[6] Superconducting and Other Innovative Materials and Devices Institute, National Research Council (CNR-SPIN), Department of Physical and Chemical Science, University of L'Aquila, 67100 L'Aquila, Italy
[7] Bioengineering Unit, Fondazione Toscana G. Monasterio, 56124 Pisa, Italy; f.frijia@ftgm.it
* Correspondence: giulio.giovannetti@cnr.it

Abstract: Magnetic resonance imaging (MRI) is a non-invasive diagnostic technique able to provide information about the anatomical, structural, and functional properties of different organs. A magnetic resonance (MR) scanner employs radiofrequency (RF) coils to generate a magnetic field to excite the nuclei in the sample (transmit coil) and pick up the signals emitted by the nuclei (receive coil). To avoid trial-and-error approaches and optimize the RF coil performance for a given application, accurate design and simulation processes must be performed. We describe the full-wave simulation of a Helmholtz coil for high-field MRI performed with the finite-difference time-domain (FDTD) method, investigating magnetic field pattern differences between loaded and unloaded conditions. Moreover, the self-inductance of the single loops constituting the Helmholtz coil was estimated, as well as the frequency splitting between loops due to inductive coupling and the sample-induced resistance. The result accuracy was verified with data acquired with a Helmholtz prototype for small phantom experiments with a 3T MR clinical scanner. Finally, the magnetic field variations and coil detuning after the insertion of the RF shield were evaluated.

Keywords: magnetic resonance; radiofrequency coils; Helmholtz coil; simulation; FDTD method

Citation: Giovannetti, G.; Burov, D.; Galante, A.; Frijia, F. Full-Wave Simulation of a Helmholtz Radiofrequency Coil for Magnetic Resonance Applications. *Technologies* **2024**, *12*, 150. https://doi.org/10.3390/technologies12090150

Academic Editors: Yudong Zhang, Zhengchao Dong and Dennis Douroumis

Received: 25 July 2024
Revised: 26 August 2024
Accepted: 2 September 2024
Published: 3 September 2024

1. Introduction

Magnetic resonance imaging (MRI) is one of the main medical imaging techniques employed for the non-invasive identification of pathologies and the follow up of diseases in different organs and tissues. Recent technical progress in spatial resolution and sensitivity, thanks to the deployment of higher-field clinical scanners, and the development of novel radiofrequency (RF) coils and new sequences, have ensured that this technique is widely used in different fields of medicine [1].

RF coil performance plays a significant role in image quality. For high-quality magnetic resonance images, RF coils must be able to support a large field of view (FOV) with high RF magnetic field homogeneity (and low electrical field) in transmission and achieve a high signal-to-noise ratio (SNR) in reception [2].

The Helmholtz coil is the simplest volume coil (i.e., not laying on a flat surface) to manufacture, suitable for both axial and non-axial B_0 MRI devices, due to possible sample insertion along its axial direction or orthogonally to it. Within such a simplified approach, it is often used for both transmission and reception. It produces, in the central region, a highly homogeneous magnetic field along the coil axis with a relatively high SNR. Generally, it is

constituted by two identical and coaxial circular loops with in-phase currents flowing in each loop, with the distance between loops equal to the loops' radius [3].

Recently, a transmit/receive Helmholtz coil was designed for MR studies in small samples with a clinical 3T scanner [4], while a Helmholtz coil paired with a V-shaped structure was proposed for the imaging of dogs in a V-shape permanent MRI system [5]. A high-temperature superconducting (HTS) probe for magnetic resonance microscopy at 400 MHz was designed as a Helmholtz pair configuration, able to provide a larger FOV and enhanced magnetic field homogeneity over a single-coil design [6]. Another work [7] suggested the design of a 0.2 T MRI scanner based on a Helmholtz coil as the main magnet, able to reduce both the weight and the cost of the system compared to equivalent permanent magnet MRI scanners. Recently, Helmholtz-like configurations constituted by a couple of transverse coils (butterfly and figure-of-eight geometries) separated by a given distance were proposed for achieving high sensitivity in a larger depth interval than in a single-sided configuration [8]. All the previously described Helmholtz coil configurations were designed and simulated by using the magnetostatic numerical integration of the Biot–Savart law, which calculates the B_1 field distribution in free space (unloaded coil) [9]. This approach is often accurate in the low-frequency regime but has three main limitations: (i) from a coil builder's perspective, it does not include the sample's effect on the coil itself (i.e., change in the tuning/matching capacitors); (ii) from an application perspective, especially regarding larger magnetic fields, the actual magnetic field distribution inside the sample can be different; and (iii) at high magnetic fields, a proper SNR calculation needs to take into account the sample's noise.

A Helmholtz coil can be used in applications to image local body districts in a human body or perform MRI experiments on small phantom and animal samples. We focused on high-field MRI applications, choosing a working field of 3 T, widely used for research applications, and an insertion bore of approximately 10 cm suitable for human limbs, as well as preclinical imaging. Despite a geometrically equivalent birdcage coil having better theoretical magnetic field homogeneity than a Helmholtz coil [10], the need to use a large number of capacitors for tuning, matching, and quadrature balancing makes it more complex to achieve. Differences in capacitor values can also break the desired discrete rotational symmetry in the birdcage and introduce unwanted field inhomogeneity [11].

In this paper, we describe the simulation of a Helmholtz coil performed with the finite-difference time-domain (FDTD) method [12]. The full-wave numerical tool permits the estimation of the B_1 magnetic field pattern for both the unloaded and loaded conditions, with the latter providing the information of how the magnetic field is affected by the electromagnetic properties of the sample. Moreover, since at high field strengths, the sample losses can be dominant with respect to the coil losses [13,14], sample-induced resistance was estimated. Finally, the single-loop self-inductance and the frequency splitting between loops were calculated. The full-wave simulation result accuracy was verified with a Helmholtz coil prototype, previously tested at the workbench and designed to be used in transmit/receive mode with a 3T clinical scanner [4]. Finally, the magnetic field inhomogeneity and coil detuning after the RF shield insertion were calculated.

2. Materials and Methods

Two identical loops sharing the same axis (z) with equal and in-phase currents have, at isocenter, zero as the magnetic field first derivative along the z-axis due to the configuration symmetry. If the loops' radii are equal to the distance between the two loops, then the structure becomes a Helmholtz coil. It produces a highly homogeneous B_1 field along the coil axis, because the magnetic field second derivative with respect to z is nulled at the isocenter. This is the Helmholtz configuration that we considered.

2.1. FDTD Simulations

Full-wave simulations were performed with the FDTD method using the commercially available software XFdtd 7.8 (Remcom, State College, PA, USA), which permits the

simulation of coils with arbitrary geometries. In this work, a single loop and a Helmholtz coil were designed using the geometry workspace of the XFdtd tool. Simulations were performed by modeling the coils with a circular section (wire) of 4 mm in diameter. From a previous work, we had indications that the Ohmic losses were negligible compared to the sample losses [4]. To verify the above finding in numerical simulations, we used a perfect electric conductor (PEC) instead of copper. In the sample's presence, the numerical agreement between the experimental and simulated data provides indirect confirmation of the loss hierarchy. An adaptive non-uniform mesh, finer in the coil conductor's proximity, was employed to minimize the computational time and load while achieving a good degree of accuracy. Perfectly matched layer (PML) boundary conditions were employed [15] to truncate outward waves and mimic an infinite computational domain.

2.2. Self and Mutual Inductance from Simulations

The simulated Helmholtz coil is constituted by two coaxial circular loops, each with an RF port (Figure 1a). We measured the inductance L of each loop (5.25 cm median radius and 2 mm wire conductor radius) by using two different approaches.

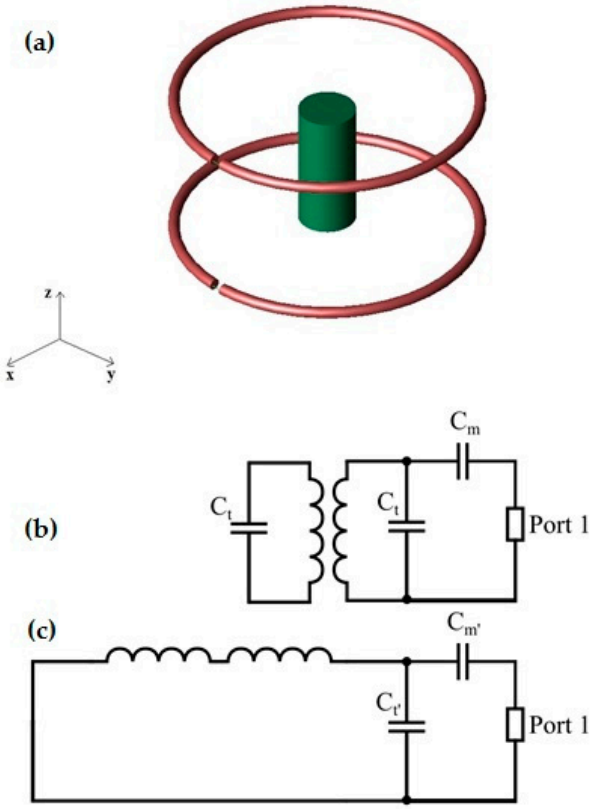

Figure 1. (**a**) Sketch of the loaded Helmholtz coil for magnetic field pattern calculations; electrical schemes for (**b**) mutual coupling configuration and (**c**) series configuration.

From an electrical point of view, a Helmholtz coil can be created in two ways: (i) with two identical resonant loops inductively coupled and with a single port on one of the two (Figure 1b), or (ii) with two identical loops connected in series, forming a single resonant circuit with a single port (Figure 1c). Within the first approach, we must consider the coupling effects among the resonators, and knowledge of self and mutual inductances is crucial to fast prototyping.

To address the first approach, a tuning capacitor C was inserted into an isolated loop, achieving a resonant circuit fed by an ideal current port. A Gaussian broadband pulse excitation in the feed port induced a damped voltage oscillation in the capacitor, which permitted the evaluation of the resonance frequency, hence the loop inductance. In the

second approach, a 50 Ω port was inserted, feeding the purely inductive isolated loop with a sinusoidal current of frequency equal to the desired Larmor frequency (f_0 = 127.75 MHz for 3 T proton MRI). The inductance was estimated from the impedance measurement performed by the simulation software [16].

When the two resonant loops are placed in proximity, although they are initially tuned to the same frequency, $f_0 = 1/2\pi\sqrt{LC}$, the inductive coupling splits this frequency into two distinct resonant modes, which differ in the phase of the current flowing in each loop.

By defining M as the mutual inductance between the two identical loops, the lower resonant frequency can be calculated as follows [17]:

$$f_L = \frac{1}{2\pi\sqrt{(L+M)C}} \tag{1}$$

(symmetric mode), which corresponds to equal and in-phase currents in the loops, useful in achieving the Helmholtz condition. Conversely, the upper resonant frequency can be evaluated as follows:

$$f_H = \frac{1}{2\pi\sqrt{(L-M)C}} \tag{2}$$

(anti-symmetric mode), corresponding to equal but 180° out-of-phase currents flowing in the two loops. In the latter case, when the distance between the two loops is equal to to $\sqrt{3}$ times the radius of the loops (Maxwell condition), the magnetic field is linear along the coils' axis (the first and third derivatives of the magnetic field with respect to z are nulled at the center) [11].

In this work, the Helmholtz coil magnetic field B_1 distribution was estimated by using a sinusoidal input current (with 1A amplitude) with the symmetric mode tuned to the Larmor frequency ($f_L = f_0$). Magnetic field patterns were evaluated both for the unloaded and loaded coil, with the load constituted by a cylindrical vial (4.5 cm long and 2 cm diameter) of high-resistivity (18.2 MΩ cm) distilled deionized water (relative dielectric constant ε = 80). We used distilled water instead of the more common saline solution for a direct comparison with the results obtained with the (computationally much faster) vector potential calculation (VPC) method based on the magnetostatic approach [4].

2.3. Sample-Induced Resistance from Simulations

The calculation of the sample-induced resistance was performed with resonant circuit theory [18] by preliminarily estimating the coil quality factor Q according to its definition: the ratio between the energy stored at the *i*-th cycle and the energy lost at the *i*-th cycle. By perturbing the coil with a Gaussian pulse (Figure 2a), we cause a voltage oscillation damped by the losses (Figure 2b). The energy stored by a capacitor is proportional to the square of the voltage across it, and the Q value is calculated as follows:

$$Q = 2\pi\frac{V_i^2}{V_i^2 - V_{i+1}^2} \tag{3}$$

where V_i and V_{i+1} represent, respectively, the voltage at the *i*-th and at the $(i + 1)$-th cycles. By performing the full-wave simulation with a PEC coil, the energy is dissipated only by the sample and radiation losses. For the sizes and frequencies involved, the latter is negligible compared to the former [19] and the sample-induced resistance R_{sample} can be calculated as follows:

$$R_{sample} = \frac{2\pi f_0 L_{tot}}{Q} \tag{4}$$

where f_0 is the resonant frequency and L_{tot} is the coil total inductance, which is the sum of each coil series inductance and the mutual inductance term as $L_{tot} = 2(L + M_{tot})$ [17], where the mutual inductance term considers both the mutual inductance between the two coils and the coil–sample mutual inductance (equal for the two loops for a uniform sample centered at z = 0).

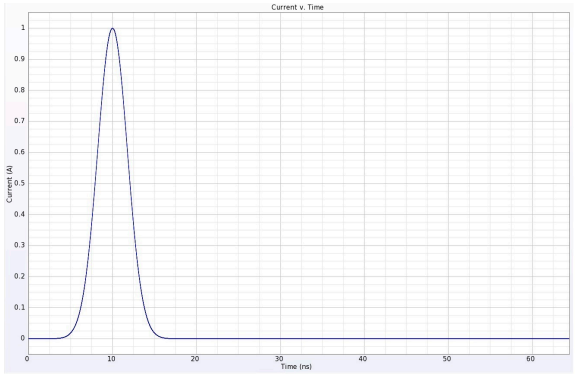

Figure 2. Quality factor evaluation for sample-induced resistance estimation: (**a**) current vs. time for the Gaussian pulse coil perturbation and (**b**) resulting potential vs. time oscillation.

This numerical approach to sample-induced resistance calculation was previously validated with experimental measurements performed on different coil–sample setups and at various resonant frequencies [20,21].

Simulation was performed with a load constituted by a $12 \times 12 \times 4.25$ cm^3 rectangular parallelepiped, the dielectric properties of which ($\sigma = 0.6$ S m^{-1}, $\varepsilon = 80$) met the American Society for Testing and Materials (ASTM) criteria for MR phantom developing [22]. The phantom dimensions were chosen, with the transversal extension larger than the loops and the longitudinal extension able to fill all the available space among the loops, in order to take into account the worst-case condition. The distance between the loop planes and the phantom was 5 mm (Figure 3).

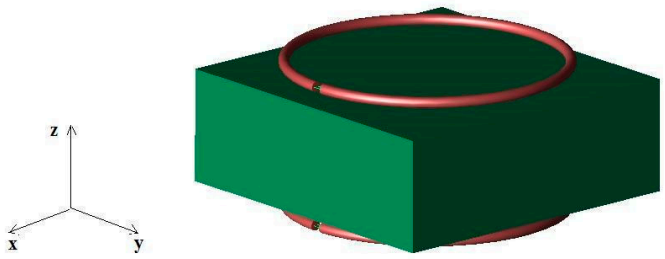

Figure 3. Sketch of the loaded Helmholtz coil for sample-induced resistance calculation.

2.4. Shielded Helmholtz Coil Simulations

The RF coil's performance can be degraded by the interaction with nearby conductive elements (cryostat, gradient and shimming coils, and permanent magnetization material). Interaction can change the coil's tuning frequency and/or matching, reduce the RF field,

and introduce extra losses. A common approach is to partially enclose the RF coil in a shield to minimize such interactions [23].

The shield itself strongly modifies the RF coil resonance frequency and magnetic field distribution while making the coil virtually insensitive to the insertion into the scanner, thus allowing an easier and faster setup (no need for in-place retune/rematch). We used the FDTD method to predict the resonance frequency shift for a different shield's radii with respect to the Helmholtz coil size, to provide useful information for the coil's builder. Simulations were performed by approximating the shield as a cylindrical surface [24] constituted by PEC with 1 mm thickness and 10 cm length, the radii of which were set to be equal to 1.2, 1.5, and 2.0 times the Helmholtz radius (Figure 4).

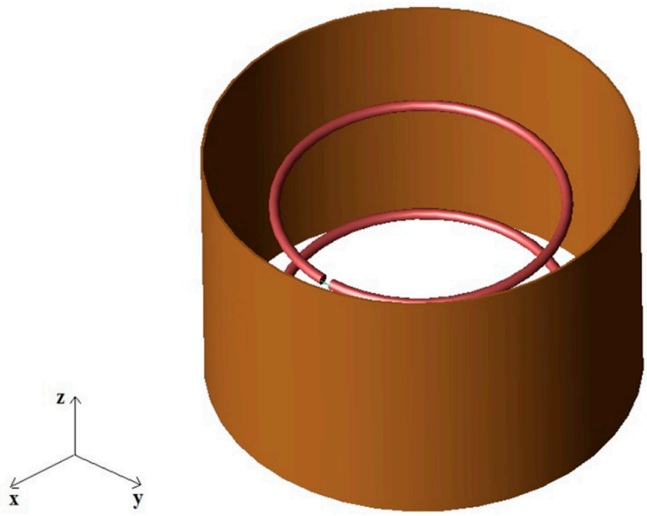

Figure 4. Sketch of the shielded Helmholtz coil.

2.5. Coil Prototype

We initially built two circular loops (5.25 cm median radius and 2 mm wire conductor radius). Before the insertion of capacitors, the loop inductance L was measured at 127.75 MHz with workbench instrumentation consisting of a network analyzer HP3577 (Hewlett Packard, Palo Alto, CA, USA) by connecting the loop to the analyzer with an RG58 coaxial cable after performing a proper calibration. Each loop was then tuned to 127.75 MHz using a variable capacitor (the capacitance of which was fixed at 6.6 pF, as measured by an impedance meter at 1 kHz). Successively, these two resonant loops were positioned at a distance equal to their radius (d = 5.25 cm). Finally, we adopted the second approach previously described, by connecting these loops in series, forming a single resonant circuit with a single port and then achieving a transmit/receive Helmholtz coil for ^{1}H MR small phantom studies with a 3T MR clinical scanner [4] (Figure 5). Coil fine-tuning at 127.75 MHz was performed with fixed and variable capacitors. For both the two separated loop and the Helmholtz structures, workbench measurements were performed with the same network analyzer, using a homemade dual-loop probe constituted by two pickup circular loops, which were partially overlapped to minimize the mutual inductive coupling between the loops; this was achieved by separating the loop centers by 0.75 times their diameter [25].

The magnetic field distribution of the Helmholtz coil prototype was extracted from images acquired with a 3T GE TWINSPEE HDxt (GE Healthcare, Waukesha, WI, USA) MR clinical scanner. In the imaging experiment, the cylindrical phantom was placed at the coil's center, with its longitudinal axis parallel to the Helmholtz coil main axis, and a sagittal image of the phantom was acquired using a fast spin echo (FSE) sequence (FOV = 80 × 80 mm, 224 × 224 matrix, slice thickness = 2 mm, TE/TR = 70 ms/2800 ms, flip angle = 90°, number of averages = 12) [4]. With the phantom being highly homogeneous, the coil magnetic field profiles can be directly estimated from the pixel values in the

acquired images, since, as with volume coils, the expected B_1 slowly varies across the imaging volume [26].

Figure 5. The Helmholtz coil prototype.

3. Results

3.1. Helmholtz Coil Simulation and Workbench Test

Both simulation methods described in Section 2.2 provided an inductance value L of 239 nH for the single loop, while the measured value for the built single loop was 235 nH [4].

The simulation of the structure constituted by the two separated single loops (without a sample) allowed us to verify the splitting resonant frequency phenomenon. The simulated higher (H) and lower (L) resonant frequencies of this structure were shown to be f_H = 135.76 MHz and f_L = 120.95 MHz, and the measured frequencies were f_H = 136.02 MHz and f_L = 120.58 MHz [4]. From Equation (1) and the simulation results, we extracted the theoretical value of the mutual inductance M, which was shown to be 27 nH, while the same equation and workbench measurement results allowed us to estimate the experimental value, was was 29 nH.

Sample-induced resistance was evaluated with numerical simulations with a parallelepiped load, using Equation (4). The sample-induced resistance value was 32 Ω, very similar to the value previously calculated with the VPC method (31 Ω) [4].

We checked that, for the working frequencies, the differences among $B_1^{-/+}$ and $|B_1|$ were negligible, and we reported the latter. The results presented in Figure 6 correspond to the coil operating at f_L, so that the current in both loops is in phase. In particular, Figure 6a,c show the simulated modulus of the B_1 field maps of the Helmholtz coil in the x–y plane at z = 0 cm (at half of the distance between the loops), and within a longitudinal section of the Helmholtz coil at x = 0 cm, respectively. Figure 6b,d depict the field plot along the *y*-axis for z = 0 cm and x = 0 cm, and the field profile along the z axis for x = 0 cm and y = 0, respectively.

3.2. Helmholtz Coil MRI

The magnetic field homogeneity of the Helmholtz coil was measured by extracting the signal intensity profile along each axis in the cylindrical phantom (Figure 1) MRI acquisition (Figure 7a,c). The experimental results (solid line) were compared with the loaded coil simulation (dashed line), shown in Figure 7b,d.

3.3. Shielded Helmholtz Coil

To compare the magnetic field homogeneity of the Helmholtz coil with different shield radii, we calculated the profiles of the B_1 field along the coil axis; see Figure 8.

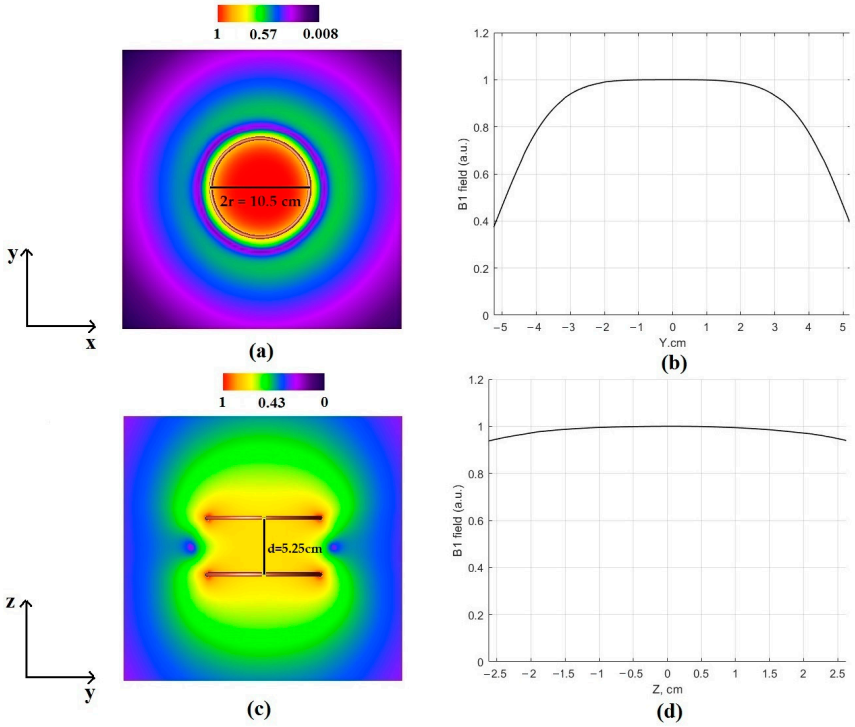

Figure 6. Modulus of the B_1 magnetic field (a.u.): in the x–y plane at z = 0 cm (**a**), along the y axis for z = 0 cm and x = 0 cm (**b**), in the y-z plane at x = 0 cm (**c**), and along the z axis for x = 0 cm and y = 0 cm (**d**).

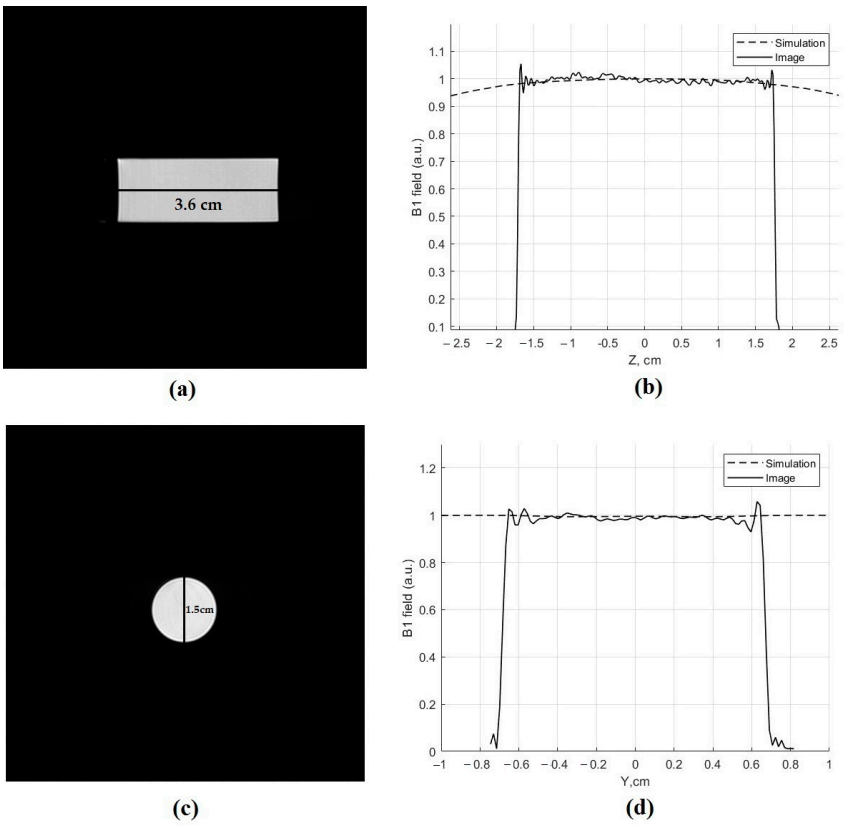

Figure 7. Phantom image in the sagittal (**a**) and axial (**c**) planes: the black lines in (**a**,**c**) were used to extract the signal intensity reported in (**b**,**d**), together with the simulated values (solid and dashed lines, respectively).

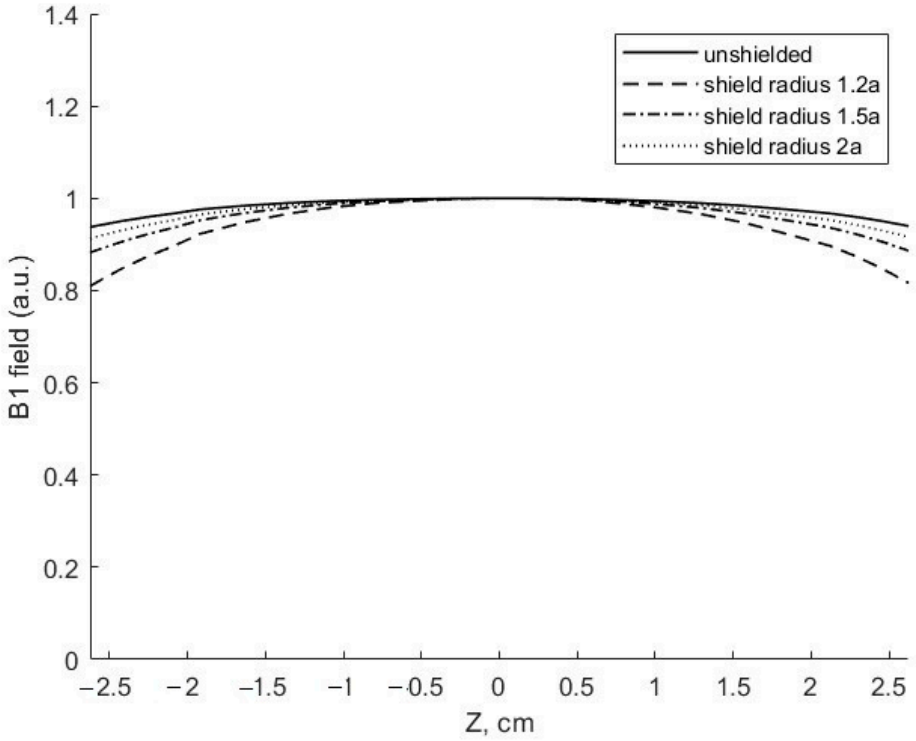

Figure 8. Overplot of the simulated B_1 magnetic field (normalized to 1 at maximum) for the Helmholtz coil (radius a = 5.25 cm) with different shield radii.

Table 1 summarizes the simulation results for the Helmholtz coil resonance frequency when a shield of different radius is considered, as well as the resultant z-axis inhomogeneity within the considered 5 cm region of interest.

Table 1. Simulation results for resonant frequencies and field inhomogeneity in the Helmholtz coils with different shield radii with respect to the coil radius a.

Shield Radius	f_L (MHz)	f_H (MHz)	B_1 Inhomogeneity (%)
Unshielded	120.95	135.76	6
2·a	126.68	137.11	9
1.5·a	135.28	141.06	12
1.2·a	154.64	156.39	19

4. Discussion

The electromagnetic tool predicted the single loop's self-inductance L with great accuracy: we measured a difference of only 1.7% with respect to the experimental value. For the Helmholtz coil configuration, built with the two resonant loops, the simulated resonant frequencies f_H and f_L showed excellent agreement with the measured values, with a deviation of only 0.2 and 0.3% for f_H and f_L, respectively.

The simulator code allowed the estimation of the sample-induced resistance by using an algorithm based on resonant circuit theory, which provided results very similar to those obtained using the VPC method. However, with respect to this last method, the algorithm allows the estimation of sample-induced resistance for systems with various geometries, without approximations in sample geometry [21].

Regarding the coil magnetic field pattern, as can be observed from Figure 6c,d, it is very homogeneous along the coil axis. The decrease in the radial direction (Figure 6a,b) is a feature already present, in vacuum, in the magnetostatic limit, as can be easily confirmed by

computing the field profile using the Biot-Savart approximation. Moreover, by comparing the plots of the simulated magnetic field for the loaded coil with those obtained from the experimental acquisition (Figure 7b,d), it is possible to verify the great accuracy of the full-wave simulation, the discrepancies in which are mainly due to experimental noise or imaging artifacts (Gibbs ringing).

The insertion of the RF shield allows the evalution of frequency splitting and magnetic field homogeneity (as well as its absolute strength variation) as a function of the shield radius. As shown in Figure 8, the presence of the RF shield impacts the magnetic field distribution. According to the imaging method [3,11], the currents induced on an RF shield are equal in intensity and position (along the z-axis in our case) to the ones flowing in the loops. The field generated by the image currents (secondary field) is less than the field generated by the loop currents (primary field) because of the larger radius of the RF shield. At the same time, the image currents do not respect the geometrical Helmholtz condition (with the same distance as the primary currents but a different radius). Therefore, the resulting field expressed as the sum of the primary and secondary one is less homogeneous than without the RF shield. When the RF shield becomes closer to the coils' radius, the secondary field becomes more homogeneous (the image currents approach the Helmholtz condition) but the total field is less intense. With our simulation, we verified that for RF shield radii in the [1.2a, 2a] radius, the effect on B_1 homogeneity is monotonic (see Table 1). Moreover, Table 1 shows the shield effect on the resonant frequencies: the insertion of the shield involves a reduction in inductance values and, therefore, the resonant frequencies increase. The proposed simulation tool can be applied to the design of different geometry coils, both in linear and circular polarization, since the FDTD algorithm allows us to incorporate complex structures, such as a part of the human body, into the computational space without limitations in the sample and coil geometries. Moreover, the proposed simulator is accurate for all frequencies routinely used in MR applications. However, for sample-induced resistance estimation, the computational time required for simulating low-frequency-tuned coils could become large with respect to the time guaranteed by the VPC, especially for simple sample–coil geometries [27].

5. Conclusions

In this paper, we proposed a simulation tool for a Helmholtz coil for high-field MRI performed with the FDTD algorithm, allowing us to evaluate the magnetic field pattern in loaded and unloaded conditions. Moreover, both the single-loop self-inductance and the frequency splitting between loops were calculated, as well as the sample-induced resistance. All theoretical results were verified via comparison with data acquired with a Helmholtz prototype designed for small phantom experiments with a 3T MR clinical scanner. Furthermore, the magnetic field homogeneity and coil detuning after the RF shield insertion were evaluated. Future developments will address the simulation of different structures constituted by two or more coil pairs for further improvement of the magnetic field uniformity.

Author Contributions: Conceptualization, G.G. and F.F.; methodology, G.G., D.B., A.G. and F.F.; software, G.G., D.B. and F.F.; validation, G.G., D.B., A.G. and F.F.; writing—original draft preparation, G.G., A.G. and F.F.; writing—review and editing, G.G., D.B., A.G. and F.F.; visualization, G.G. and F.F. All authors have read and agreed to the published version of the manuscript.

Funding: Denis Burov acknowledges the EC MSCA-DN FC-RELAX project (GA 101072758) for financial support.

Data Availability Statement: Dataset available on request from the authors.

Conflicts of Interest: Author Denis Burov was employed by the company Stelar s.r.l. The remaining authors declare that the research was conducted in the absence of any commercial or financial relationships that could be construed as a potential conflict of interest.

References

1. Asher, K.; Bangerter, N.K.; Watkins, R.D.; Gold, G.E. Radiofrequency Coils for Musculoskeletal MRI. *Top. Magn. Reson. Imag.* **2010**, *21*, 315–323. [CrossRef] [PubMed]
2. Haase, A.; Odoj, F.; Von Kienlin, M.; Warnking, J.; Fidler, F.; Weisser, A.; Nittka, M.; Rommel, E.; Lanz, T.; Kalusche, B.; et al. NMR probeheads for in vivo applications. *Conc. Magn. Reson.* **2000**, *12*, 361–388. [CrossRef]
3. Mispelter, J.; Lupu, M.; Briguet, A. *NMR Probeheads for Biophysical and Biomedical Experiments: Theoretical Principles & Practical Guidelines*, 2nd ed.; Imperial College Press: London, UK, 2015.
4. Giovannetti, G.; Frijia, F.; Flori, A.; Montanaro, D. Design and Simulation of a Helmholtz Coil for Magnetic Resonance Imaging and Spectroscopy Experiments with a 3T MR Clinical Scanner. *Appl. Magn. Reson.* **2019**, *50*, 1083–1097. [CrossRef]
5. Bin, M.; Kai-Wen, H.; Wei-Min, W. A novel radio frequency coil for veterinary magnetic resonance imaging system. *Chin. Phys. B* **2010**, *19*, 076103. [CrossRef]
6. Hurlston, S.E.; Brey, W.W.; Suddarth, S.A.; Johnson, G.A.; Fitzsimons, E.G. A high-temperature superconducting Helmholtz probe for microscopy at 9.4 T. *Magn. Reson. Med.* **1999**, *41*, 1032–1038. [CrossRef]
7. Ghosh, S.K.; Thakur, V.; Chowdhury, S.R. Design and simulation of Helmholtz coil and Maxwell coil for low cost and low magnetic field MRI machine. *Adv. Mater. Proc.* **2017**, *2*, 802–806.
8. Giovannetti, G.; Alecci, M.; Galante, A. Magnetostatic Simulation and Design of Novel Radiofrequency Coils Based on Transverse Field Current Elements for Magnetic Resonance Applications. *Sensors* **2024**, *24*, 237. [CrossRef]
9. McVeigh, E.R.; Bronskill, M.J.; Henkelman, R.M. Phase and sensitivity of receiver coils in magnetic resonance imaging. *Med. Phys.* **1986**, *13*, 806–814. [CrossRef]
10. Derby, K.; Tropp, J.; Hawryszko, C. Design and eval-uation of a novel dual-tuned resonator for spectroscopic imaging. *J. Magn. Reson.* **1990**, *86*, 645–651.
11. Jin, J. *Electromagnetic Analysis and Design in Magnetic Resonance Imaging*; CRC: Boca Raton, FL, USA, 1999.
12. Yee, K.S. Numerical solution of initial boundary value problems involving Maxwell's equations in isotropic media. *IEEE Trans. Antenna Propag.* **1966**, *14*, 302–307.
13. Hoult, D.I.; Richards, R.E. The signal-to-noise ratio of the nuclear magnetic resonance experiment. 1976. *J. Magn. Reson.* **2011**, *213*, 329–343. [CrossRef] [PubMed]
14. Hoult, D.I.; Lauterbur, P.C. The sensitivity of the Zeumatographic Experiment Involving Human Samples. *J. Magn. Reson.* **1979**, *34*, 1425–1433.
15. Duan, Y.; Ibrahim, T.S.; Peterson, B.S.; Liu, F.; Kangarlu, A. Assessment of a PML Boundary Condition for Simulating an MRI Radio Frequency Coil. *Int. J. Antennas Propag.* **2008**, *2008*, 563196. [CrossRef]
16. Giovannetti, G.; Frijia, F.; Flori, A.; Galante, A.; Rizza, C.; Alecci, M. A Practical Guide to Estimating Coil Inductance for Magnetic Resonance Applications. *Electronics* **2022**, *11*, 1974. [CrossRef]
17. Javor, E.R.; Anderson, T. Design of a helmholtz coil for low frequency magnetic field susceptibility testing. In Proceedings of the International Symposium on Electromagnetic Compatibility, Denver, CO, USA, 24–28 August 1998; pp. 912–917.
18. Giovannetti, G.; Viti, V.; Liu, Y.; Yu, W.; Mittra, R.; Landini, L.; Benassi, A. An accurate simulator for magnetic resonance coil sensitivity estimation. *Conc. Magn. Reson. Part B Magn. Reson. Eng.* **2008**, *33*, 209–215. [CrossRef]
19. Lemdiasov, R.A.; Obi, A.A.; Ludwig, R. A numerical postprocessing procedure for analyzing radio frequency MRI coils. *Conc. Magn. Reson. Part A* **2011**, *38*, 133–147. [CrossRef]
20. Hartwig, V.; Tassano, S.; Mattii, A.; Vanello, N.; Positano, V.; Santarelli, M.F.; Landini, L.; Giovannetti, G. Computational Analysis of a Radiofrequency Knee Coil for Low-Field MRI Using FDTD. *App. Magn. Reson.* **2013**, *44*, 389–400. [CrossRef]
21. Giovannetti, G.; Hartwig, V.; Landini, L.; Santarelli, M.F. Sample-induced resistance estimation in Magnetic Resonance experiments: Simulation and comparison of two methods. *App. Magn. Reson.* **2011**, *40*, 351–361. [CrossRef]
22. *ASTM F2182-11a*; Standard Test Method for Measurement of Radio Frequency Induced Heating near Passive Implants during Magnetic Resonance Imaging. American Society for Testing and Material (ASTM) Designation: West Conshohocken, PA, USA, 2004.
23. Vaughan, J.T.; Griffiths, J.R. *RF Coils for MRI*; Wiley: Hoboken, NJ, USA, 2012.
24. Jin, J.; Magin, R.L.; Shen, G.; Perkins, T. A Simple Method to Incorporate the Effects of an RF Shield into RF Resonator Analysis for MRI Applications. *IEEE Trans. Biomed. Eng.* **1995**, *42*, 840–843. [PubMed]
25. Roemer, P.B.; Edelstein, W.A.; Hayes, C.E.; Souza, S.P.; Mueller, O.M. The NMR phased array. *Magn. Reson. Med.* **1990**, *16*, 192–225. [CrossRef]
26. Giovannetti, G.; Viti, V.; Positano, V.; Santarelli, M.F.; Landini, L.; Benassi, A. Coil sensitivity map-based filter for phased-array image reconstruction in Magnetic Resonance Imaging. *Int. J. Biomed. Eng. Technol.* **2007**, *1*, 4–17. [CrossRef]
27. Saydam, T.; Aksoy, S. Error analyses of the two-equations two-unknowns method for low-frequency FDTD problems. *J. Comput. Electron.* **2020**, *19*, 1573–1578.